

# 6

---

## Dreaming of the future: The 2004 Venus transit

For the first time ever, the Venus 2004 transit provided the opportunity to test the technique called *Transit Spectroscopy*, in a planet whose atmosphere is better known than those of the planets orbiting another stars. In this chapter we describe infrared spectroscopy of the 2004 Venus transit taken at the Vacuum Tower Telescope (VTT) located at the Observatorio del Teide, which allowed to detect  $^{12}\text{CO}_2$  and  $^{13}\text{CO}_2$  absorption lines in its atmosphere, thus demonstrating the capabilities of the technique.

### 6.1 Introduction

IN June 2004, Venus passed in front of the solar disk, producing a transit of a solar planet. This alignment only occurs typically twice every century, the previous one having occurred in 1882. There is an important difference with the more frequent Mercury transits: the dense Venus atmosphere. At the Venus limb position, the light coming from the solar disk will be blocked by the atmosphere at those wavelengths in which the opacity of the atmospheric components is high. Measuring the ratio between the solar spectra in a region where there is no Venus atmosphere and in a region with atmosphere will thus provide clues about the components of the atmosphere and their temperatures and densities. We saw in the Introduction the basics of this technique and its application to the transiting planet HD 209458b. On this occasion, the atmosphere of the planet has been studied and measured from ground and space

probes, and thus the findings with transit spectroscopy can be directly compared and checked with the current knowledge of its atmosphere. We planned the observations of the Venus transit to not only validate the technique, but also provide some information on a poorly-known region in the Venus atmosphere: the mesosphere.

### 6.1.1 The Venus mesosphere

The Venus mesosphere is a transition region which separates the thermosphere, with a subsolar to antisolar (SSAS) wind regime, at altitudes above  $\sim 120$  km (Bougher et al. 1997) from the troposphere, with an intense zonal retrograde flow (below 60 km altitudes or 250 mbar, Gierasch et al. 1997). The first measurements of this region were derived from Pioneer Venus observations (Taylor et al. 1980), and revealed an inverted equator-to-pole temperature gradient at 70 to 100 km ( $p=3\times 10^{-5}$  bar), which was associated with the decay of the cloud-top (located at  $\sim 65$  km altitude) super-rotation. The mesospheric temperature varies from  $\sim 240$  K at 60 km down to  $\sim 170$  K at 100 km, and a “cold collar” structure has been detected at  $\sim 65^\circ\text{N}$  with an associated vertical temperature inversion of  $\sim 15$  K at the morning terminator and 0-5 K at the evening. This structure has shown significant variability with time (Newman et al. 1984). Almost all the data on this region comes from spacecraft<sup>1</sup>; the only other information on this region has been obtained through visible observations of CO<sub>2</sub> lines<sup>2</sup>, 10- $\mu\text{m}$  measurements of CO<sub>2</sub> bands<sup>3</sup>, and millimeter and sub-millimeter wave CO observations<sup>4</sup>. Thus, the region between  $\sim 80$  and  $\sim 100$  km has very few observations which use the CO<sub>2</sub> spectral lines. The CO measurements are complicated by the still not well understood mechanism of photochemical production and redistribution, as suggested by a controversial

<sup>1</sup>Thermal field measurements from CO<sub>2</sub>: observations of the Pioneer Venus Orbiter Infrared Radiometer, the Venera 15 Infrared Fourier Spectrometer Experiment and the Galileo Near-Infrared Mapping Spectrometer; Temperature measurements from Radio Occultations: Pioneer Venus, Veneras and Magellan; Temperature measurements from Pioneer Venus Probe data, and wind measurements at the cloud tops obtained from tracking ultraviolet features, on the Pioneer Venus and Galileo missions; see Lellouch et al. (1997) for a complete revision on these measurements.

<sup>2</sup>These lines provide wind information of a region just above the clouds, 65-85 km. The first observations generated some controversy in the late 1970s; they are finally consistent with a rapid decrease of the zonal super-rotation above the cloud tops (Young et al. 1979).

<sup>3</sup>Produced in a  $\sim 20$  km layer centered at 109 km (Deming & Mumma 1983), and dominated by the SSAS flow, with an tentative detection of the return branch of the thermospheric flow at mesospheric levels (Goldstein 1989).

<sup>4</sup>Sampling a region between 75-105 km, with vertical resolutions of 4-5 km, and allowing the detection of a *mesopause* at  $\sim 91$  km in the dayside and  $\sim 87$  km in the nightside (Clancy, Sandor, & Moriarty-Schieven 2003).

morning peak in CO abundance: it was observed to occur at  $0.6 \pm 0.6$  a.m. local time above 95 km, while it appeared shifted to  $8.5 \pm 1$  a.m. below 90 km (Clancy & Muhleman 1985); these authors needed significant retrograde zonal winds at this altitude levels to explain this distribution, which has been criticized by Goldstein (1989), and also contradicts the conclusions of the Young et al. (1979) work.

The few wind velocities measurements show SSAS wind velocities at the Venus terminator (and altitudes around 100 km) in the range 105-140 m/s (typical uncertainties of 15-20 m/s, Goldstein et al. 1991, Betz et al. 1977), while the retrograde zonal flow is not so well constrained at the upper mesosphere-lower thermosphere altitudes (there are reported values from +5 m/s, thus a prograde flow, Goldstein et al. 1991, to -90 m/s, Goldstein 1989, Betz et al. 1977); this strong variability in the reported values is suspected to be related to wave activity (Bougher et al. 1997).

The mesosphere is thus a transition region in which the retrograde zonal flow observed at the cloud tops is expected to decrease with altitude, while the SSAS thermospheric flow behavior gets more important. But there is a lack of direct wind measurements on this region, and, as we have seen, the few observations are a matter of controversy. The transmitted spectral CO<sub>2</sub> lines in the Venus 2004 transit were expected to sample this poorly known region.

## 6.2 Observations

Four days at the Kiepenheuer Institut für Sonnenphysik's (KIS) VTT were assigned to the project, from June 5 to June 8. The Sun rose at  $\sim 06:30$  UT on the morning of June 8 with Venus already in front of the disk, and the third and fourth contacts happened at 11:07 and 11:26 UT. The VTT consists of a 46 m effective focal length, 70 cm solar telescope, equipped with an Echelle spectrograph that, when used in the infrared mode and with a slit width of  $0.4''$ , provides a resolving power of 200000. The detector used was the  $256 \times 256$  pixel Tenerife Infrared Polarimeter (TIP, Martínez Pillet et al. 1999), in the Spectrograph mode (no polarimeter). The image scale in the focal plane was of  $0.36''/\text{pixel}$ , and at the distance of Venus at the moment of transit, 200 km were translated in  $\sim 1''$ . The total field of view was  $\sim 92''$ , and the Venus disk had a maximum diameter of  $58.2''$ . In the spectral axis, the wavelength range covered at the regions around  $1.5 \mu\text{m}$  is of  $8 \text{ \AA}$ ; thus, each pixel samples a total of  $0.031 \text{ \AA}$ . Series of 50 ms exposures were accumulated to provide 1 s integration time images every  $\sim 3$  s (the rest of the time is spent by the system in writing the images to disc, reading the CCD, communicating with the telescope, etc.). All the images show a fringe pattern, a central horizontal line that divides the two

TABLE 6.1— Observing log. Spectral region *Favorite* = 1.5965-1.5973 $\mu\text{m}$ , *Grab bag* = 1.61245-1.6132 $\mu\text{m}$ , *Favorite +* = 1.5975-1.5983 $\mu\text{m}$ , Slit position 1 = 45.5°, position 2 = 315.5° (measured from the Venusian north anti-clockwise).

Time (UT)	Spectral Region	Slit position	Comments
06:51:27-06:54:10	Favorite	2	Dark images
06:57:20-07:02:17	Favorite	2	Flat field images
07:33:16-07:55:55	Favorite	2	Full scan
08:02:08-08:06:51	Grab bag	2	Flat field images
08:15:06-08:43:07	Grab bag	2	TESOS-led
08:55:25-09:00:23	Grab bag	2	Flat field images
09:10:25-09:26:32	Grab bag	2	Full scan
09:31:32-09:36:11	Grab bag	1	Flat field images
09:52:48-09:55:01	Grab bag	1	Partial scan, no AO, telescope failure at the end
10:02:51-10:24:09	Grab bag	1	Manual full scan, no AO
10:29:21-11:19:22	Favorite +	1	Manual partial scan, AO?
11:19:36-11:29:05	Favorite +	1	Manual partial scan, Venus close to limb, TESOS-led
11:30:27-11:35:09	Favorite +	1	Flat field images
11:36:07-11:40:45	Favorite +	1	Dark images

upper 128 $\times$ 128 chips from the two lower ones, and a region with a noticeable number of bad pixels in the upper-left corner (where we define the orientation as in the figures plotted further down). A gain jump between the left and right chips is also visible.

Flat field images were obtained by moving continuously the telescope through a part of the disc close to the center and without magnetic regions. These images were obtained before and after every scan of the Venus disk, and after changing the slit orientation and/or the spectral range (the fringe pattern depends on both changes). Also, to correct for the temperature dependence of the chip, sets of 30 dark images were obtained, by putting a cover in the entrance of the spectrograph.

The system is equipped with Adaptive Optics, that was used after the  $\sim$  1st hour of data acquisition, when the Sun was at a suitable altitude above the horizon. The sky conditions were very good, with a clear sky, no dust, and seeing conditions varying around 1". Several technical problems happened the morning of the transit, causing a total of  $\sim$  1 hour of lost observing time. The need for manually-controlled drift scans of the Venus disk limited the use of AO to only one of the two used slit orientations.

Three complete scans of the disc of Venus and three partial scans were obtained (see Table 6.1), in two different slit orientations and three different spectral regions close to 1.5  $\mu\text{m}$ .

### 6.3 Data analysis

In this section we describe the details of the process followed to obtain the spectral absorption lines. Two main problems in the images had to be treated carefully: the fringe pattern, which is time-dependant, and the diffuse light in

the Venus limb, which has a signal a factor of  $\sim 10$  smaller than the solar disk.

### 6.3.1 Calibration

Average flat-fields and dark currents were obtained combining typically 30 exposures of each type of image. Bad pixels are detected by subtracting each image from a 4 points smoothed image and establishing a certain threshold. Those points above or below the threshold are substituted with the smoothed value, and the process is repeated two more times, with different image smoothing and thresholds.

Even though if the images are bias-corrected at the time of storage of the images in the computers at the telescope, a division with a normalized flat-field images doesn't work properly. As seen in the subtracted image shown in Figure 6.1 (in the next subsection we'll describe how these images were obtained), whilst the fringes disappear in the solar disk, there are fringes in the venusian disk, and consequently in the limb. This is a consequence of diffuse light in the Venus disk. To investigate this diffuse light component, we made a linear fit of the minimum signal of the Venus disk as a function of its width in the image. The coefficients of this fit were used to estimate the diffuse light from the measured width of the disk in each of the images. Subtracting this value (multiplied by a constant value of around 0.45 as explained below), and flat-fielding, results in a subtracted image where, contrary as in Figure 6.1, the fringes are now evident in the part of the solar disk, and they have been successfully removed from the venusian disk (Figure 6.2). This is a consequence of the diffuse light affecting to the pixels with lower signal. Thus, we used in every image a wavelength-averaged image profile to build a "diffuse light" image that has  $\sim 0$  value in the parts with solar disk, and the diffuse light constant in the center of the venusian disk. A cut in the wavelength axis of this "diffuse light" image is plotted in Figure 6.3. The fringes are optimally removed from the final images if this diffuse light image is multiplied by a constant value before subtracting it from the data images<sup>5</sup>. Figure 6.4 plots one random subtracted image, to show that there are few remains of the fringe pattern.

---

<sup>5</sup>These constant values are different at each of the spectral regions, probably as a consequence of the different average solar continuum signal at each wavelength. The spectral regions with more solar signal will be more affected by diffuse light. For the Favorite and the Favorite + regions, this constant value is estimated as 0.45; in the Grab Bag region the fringes are better removed if a constant value of 0.25 is used.

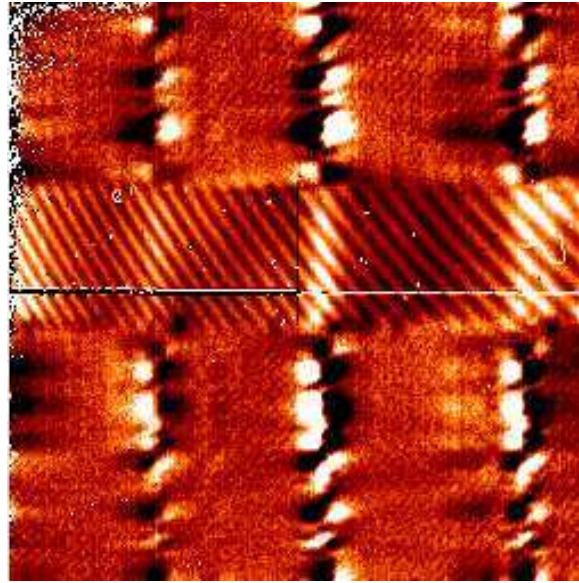


FIGURE 6.1— Difference of a flat fielded (as typically done) image and a model image (see text for details); wavelength is increasing to the right, and the central part is the Venus disk. The fringes have not been well removed from the disk.

### 6.3.2 Obtaining the spectral lines

In order to get rid of the parts that do not vary from image to image, we built, for every image, an artificial image that is the vectorial product of an average in the  $x$  direction times the average in the  $y$  direction. The subtraction of this image from the original leaves only the parts that are not common to all the images. In Figure 6.4 there are several features easily distinguishable:

- The solar spectral lines appear with positive and negative values, due to the different speeds of the plasma in the granules.
- There is still some residual fringing.
- In a few places in the Venus limb, absorption lines are clearly visible. They have not the same depth in the two limbs.

### 6.3.3 Final spectra

In every calibrated image, the ratio was built between the intensity at the limb locations (3 pixels were considered) and the intensity 11 pixels away from the

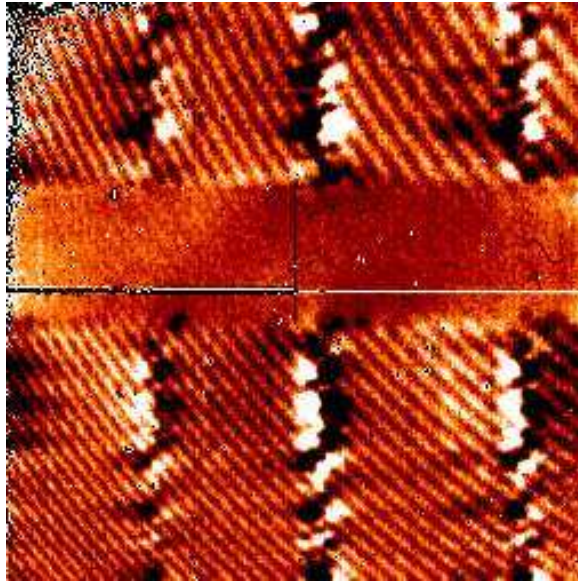


FIGURE 6.2— Same as Figure 6.1, but where a constant value has been subtracted to the image before flat fielding. Now, the fringes have been well removed from the Venus disk, but not from the Solar disk.

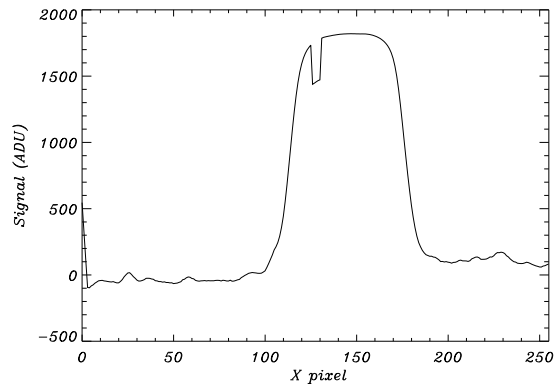


FIGURE 6.3— A vertical cut in a typical "bias" image, constructed as described in the text. It will subtract a constant value to the venusian disk, while the rest of the image will remain basically unaffected.

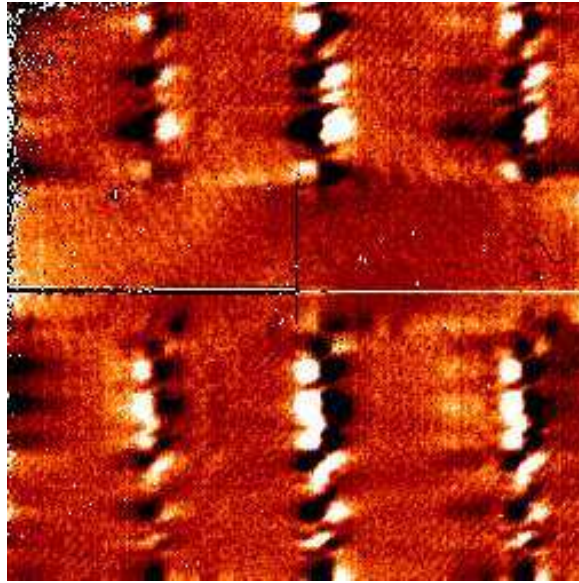


FIGURE 6.4— Final difference image, after correction with the artificial image whose cut is shown in Figure 6.3. Now, the fringes have been efficiently removed from all the image, and Venus absorption lines appear in both of the Venus limbs.

Venus disk. The ratio was normalized and corrected for gradients in the two segments of the CCD by a parabolic fit to regions of the spectra where no strong solar lines nor  $^{12}\text{CO}_2$  absorption lines were expected. A visual inspection of the subtracted images allowed to reject bad exposures, in which the telescope was being moved, or the absorption lines were not clear, due to worst atmospheric conditions. The total final spectrum in each of the spectral regions was built as the median value of all the individual spectra. The final spectra in two of the three different spectral regions are plotted in Figures 6.5 and 6.6.

Absorption features in those spectra are evident, in the expected wavelengths. All the lines seem to appear in doublets, which is due to fortuitous overlaps with the  $^{13}\text{CO}_2$  molecular absorption lines, not considered initially in the model.

The orientation of the slit at the time of third contact, in the slitjaw images, and the ephemerides for the transit impact parameter and orientation of the Solar and Venusian rotation axes were used to infer the latitude at which the two limbs were, in each of the images. This allowed to average several spectra in latitude-bins, in order to study possible differences in these. The spectral region

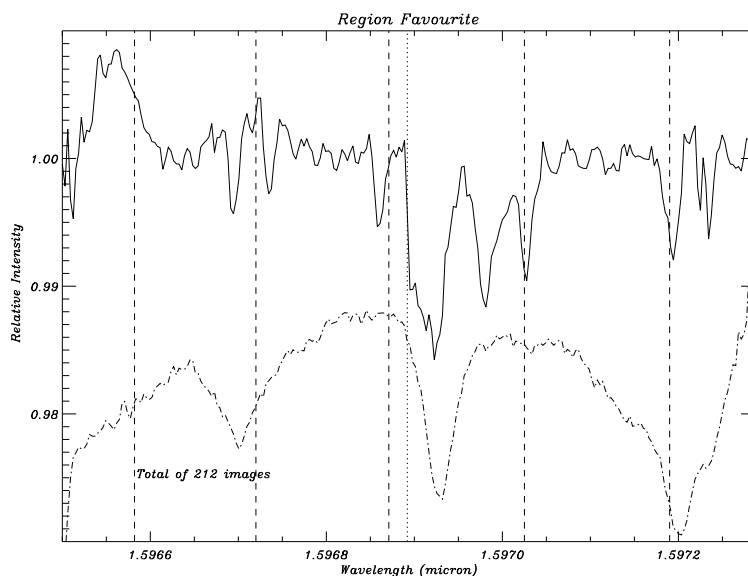


FIGURE 6.5— Final spectrum of the Favorite region, constructed as average spectra of the two limbs. Each spectra of the limbs is the median of 212 spectra, which are the ratio of the signal at 3 pixels centered on the Venus limb and 3 pixels located 11 pixels away on the solar disk. The individual spectra are fitted to a 2nd order polynomial in each of the CCD left and right halves (see text for details). Vertical dashed lines show the expected  $\text{CO}_2$  absorption features, from the model described in the Introduction. The vertical dotted line marks the division between the two left and right chips. The dash-dotted line plots the mean solar + telluric spectrum at this region. Features that appear close to strong solar + telluric lines should be considered with special care.

Favorite + was used for this purpose, as the lines are more clearly detected in this wavelength range, and  $\sim 40$  minutes were spent in a narrow set of latitudes. The Figures 6.7 and 6.8 show these binned spectra.

A total of 534 good images in the Favorite + region, sampling venusian latitudes between  $0\text{-}30^\circ$  (one limb) and  $55\text{-}85^\circ$  (the other), were used to obtain two averaged transmission spectra. These are plotted in Figure 6.9. The low-latitude absorption lines are less deep, specially the doublet close to  $1.59792 \mu\text{m}$ . Further work will be devoted to establish whether this latitude dependence is real or an instrumental effect, such as an asymmetric PSF behavior.

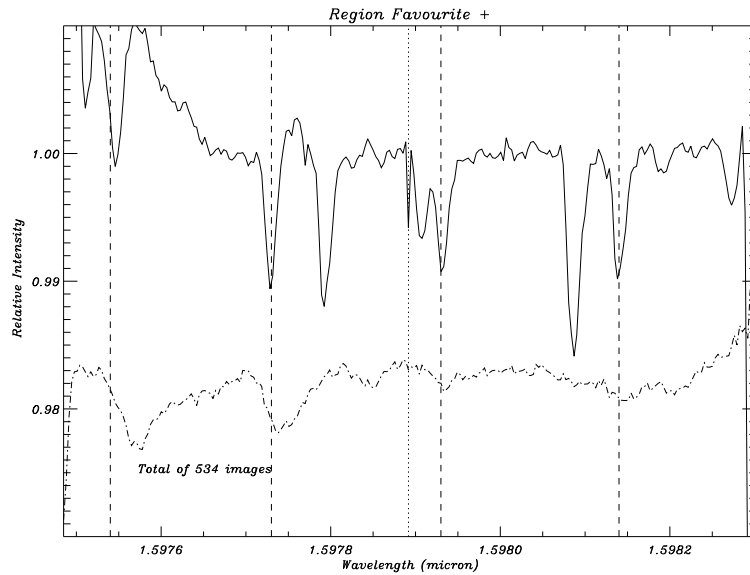


FIGURE 6.6— Same as Figure 6.5, for the Favorite + region. The S/N level of this spectrum is higher than in the other regions, due to the few solar + telluric features at these wavelengths and to the bigger amount of collected data.

#### 6.4 Summary and future improvements

The spectral signatures of  $\text{CO}_2$  have been detected for the first time as absorption features at the limbs of Venus while it is passing across the disk of the Sun. The relative strengths of the  $^{13}\text{CO}_2$  and  $^{12}\text{CO}_2$  close spectral lines have been observed to be different from the terrestrial cases, an effect that can be due to temperature differences between the terrestrial and Venusian atmospheres. Variations in the strengths of these features with the Venusian latitude of the limbs at which the slit cuts the disk of Venus are consistent with the increased temperatures at higher latitudes, an effect observed by the Pioneer Venus Orbiter for the first time.

Unfortunately, the fringes and diffuse light at the detector have placed a limitation on the expected performance of the observations. Our initial plans, to continuously rotate the slit in steps of a few (3-5) degrees, had to be changed due to the importance of the fringing on the detector, which required specific calibration images at each position of the slit, thus involving a precious amount of time. This has also limited our plans to perform a Doppler analysis of the absorption lines, which could provide information on the winds at the mesospheric

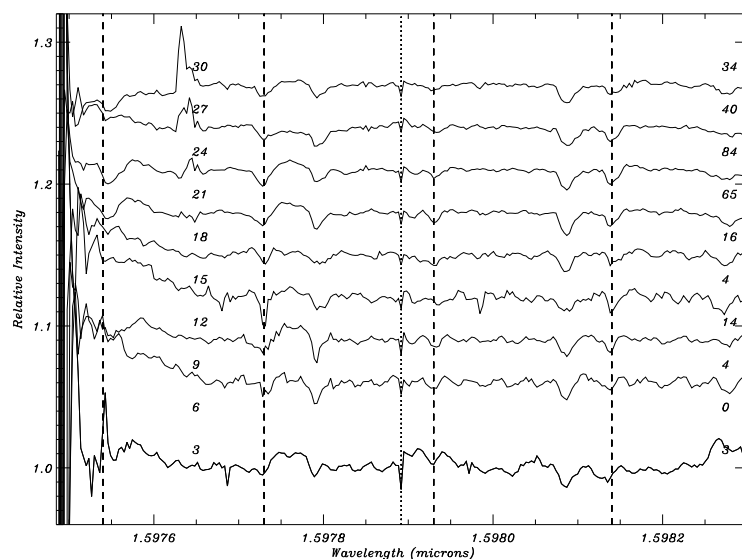


FIGURE 6.7— Latitude-binned spectra at the Favorite + region. The numbers on the left are the mean latitude of each bin, while the number on the right represents the number of averaged spectra in that bin. A total of 264 spectra have been considered. The apparent “emission lines” at  $\sim 1.59763\mu\text{m}$  and  $20\text{-}30^\circ$  are due to residual bad pixels. All latitudes are in the Northern hemisphere.

level, and at different altitudes. The S/N level of even our best averaged spectra (Figure 6.6) is not enough as to provide the minimum useful velocities precision of a few tens of m/s. The FWHM of the absorption lines in this spectrum is  $\sim 6$  pixels, which at this wavelengths translates in a Doppler shift of  $\sim 3.5$  km/s ( $v=c*\Delta\lambda/\lambda$ )

This work demonstrates the capabilities of the transmission spectroscopy to detect spectral signatures of the atmospheres of transiting exoplanets. Despite the current technical impossibility to have any spatial resolution on the host star and on the planet, and thus to make any latitude-dependant study on an exoplanet be not more than a dream for the next (several) decades, there is one important advantage of the exoplanetary transits: its more frequent occurrence. To try to repeat or improve the measurements described in this Chapter, we have to wait to the next Venus transit on June 2012, and after that to December 2117, while the transits of planets like HD 209458b or TrES-1 happen roughly every 3 days. Thus, it seems that refinements on the transit spectroscopy technique for the study of planetary atmospheres will be preceded

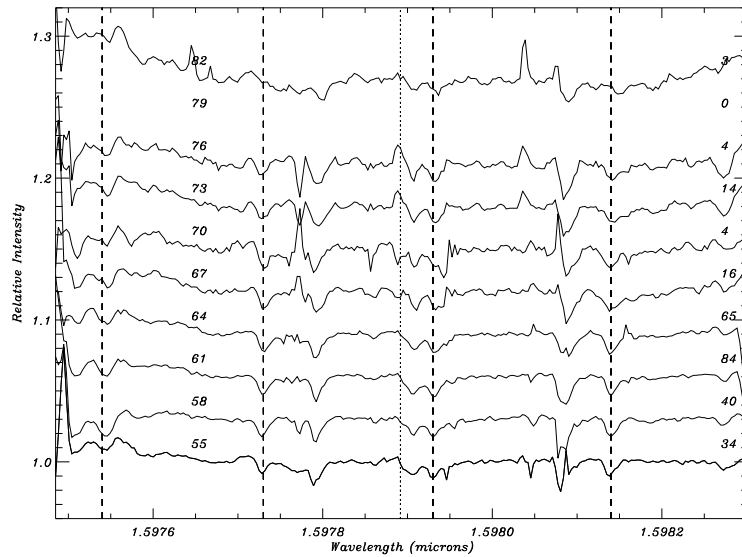


FIGURE 6.8— Same as Figure 6.7, for higher latitudes.

by the study of the exoplanet's atmospheres in the next decades.

As possible future improvements, more care could be paid to the time dependence of the fringing pattern. We noticed that it showed detectable variations after  $\sim 30$ -50 images ( $\sim 1$  minute); a way to try to reduce this variations would be to construct intermediate "flat field" images with the data. This false flat field images would show some real structure (such as granulation), but they would provide a better removal of the fringe pattern. The images where the Venus disk is small (slit almost tangential to the disk) might be used for this purpose; the fringes would not need to be optimally removed at the disk center, as only the signal at the limb and close to the limb in the solar part are used.

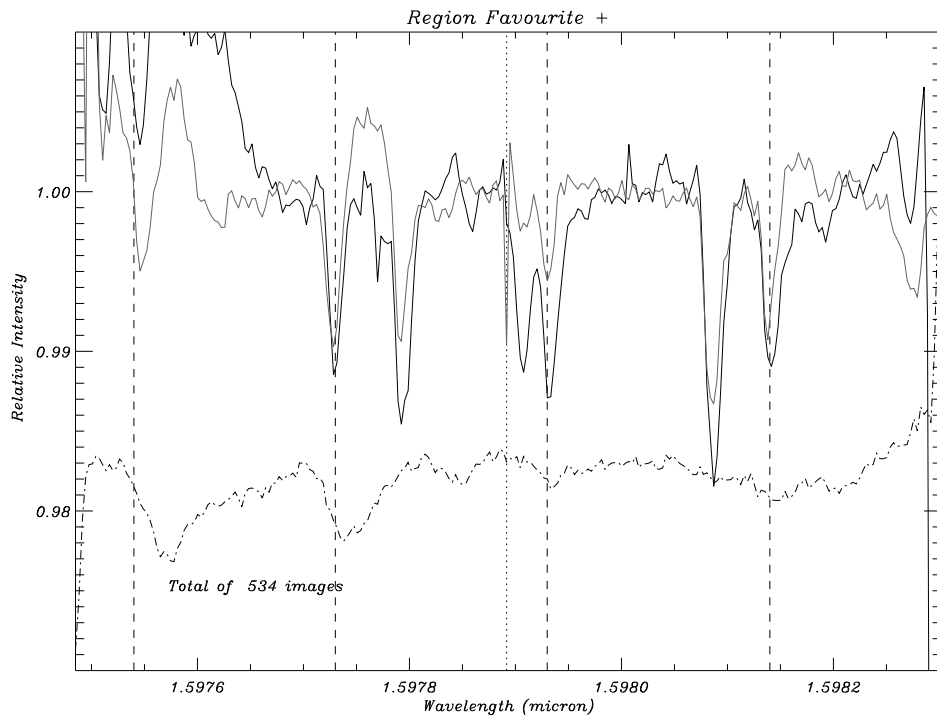


FIGURE 6.9— Median of the transmission spectra at the two limbs, separately. The solid line is for the limb at higher latitudes ( $55\text{-}82^\circ$ ) while the dotted line plots the limb located at lower latitudes ( $3\text{-}30^\circ$ ) of the venusian northern hemisphere.

